9th International Conference on Hydrodynamics
October 11-15, 2010 Shanghai, China

ELSEVIER

Available online at www.sciencedirect.com
ScienceDirect
Journal of Hydrodynamics
2010, 22(5), supplement: 960-968
DOI: 10.1016/S1001-6058(10)60059-5

www.sciencedirect.com/
science/journal/10016058

Dwarf solitary waves and low tsunamis

Sunao Murashige[1*] , Theodore Yaotsu Wu[2]
[1]School of Systems Information Science, Future University Hakodate
Hakodate, Hokkaido,Japan
[2]Engineering and Applied Science, California Institute of Technology
Pasadena, California, U.S.A
[*] E-mail: murasige@fun.ac.jp

ABSTRACT: This work applies the regularized solitary wave theory to develop accurate computational method for evaluating the dwarf solitary waves, with amplitude-to-water depth ratio $\alpha \le 10^{-2}$, as a useful model of one-dimensional tsunamis propagating in the open ocean. The algebraic branch singularities of these solitary waves magnifying with diminishing wave amplitude, making their computations insurmountable by existing methods, are removed by the regularized coordinates given by this new theory. Numerical examples show that this new method can produce accurate results even for $\alpha \cong 10^{-3}$ or less.

KEY WORDS: Regularized solitary wave theory; one-dimensional tsunami waves; flow singularities; conformal mapping; numerical computation.

1 INTRODUCTION

We continue our series of studies on the general problem of a solitary wave of height a progressing in permanent form on a layer of water of rest depth h with wave velocity c (or Froude number $F = c/\sqrt{gh}$ with gravitational acceleration g), described in steady state relative to the wave frame in the physical (x, y)-plane, for the wave of dimensionless height of $\alpha = a/h$ (see Fig.1(a)). The main objective here is focused on the group of so-called *dwarf solitary waves* of height $\alpha \le 10^{-2}$, down in scale to the tsunamis found in the open ocean which are commonly measured as low as $\alpha \cong 10^{-4}$. These waves were noted by Wu et al. [1] to lend a mounting challenge for evaluation of high accuracy, with relative error of 10^{-6} or less as that readily attained for higher waves.

Historically, the problem of solitary waves of all heights has been developed for asymptotic and exact solutions in various approaches (for a recent review of the literature, cf. Wu et al. [1]). They include power series expansions in terms of a single small parameter such as $\alpha = a/h$, for which Stokes pioneered in 1847 by introducing the method of perturbation expansion to determine the nonlinear effects in water waves to third order, and later in 1880 to fifth order for periodic waves on water of constant rest depth. This approach has been further pursued by expert mathematicians in the field, using other small parameters e.g. $\beta = \alpha/F^2$, $\gamma = F^2 - 1$ or $\varepsilon = k^2h^2$, k being the wave number (cf. Wu et al. [2]). With the expansion brought to the 25-th order by Wang and Wu [3], still no conclusion can be drawn on the convergence of the series expansion for the wave field. Another approach is by means of using some boundary integral equation for computational analysis of numerical solutions. This method has been adopted by Friedrichs and Hyers [4] for proving the existence of solitary waves. A different approach has been introduced by Wu et al. [1] to establish the so-called unified intrinsic functional expansion (UIFE) theory for evaluating solitary waves on water, as will be recited in essence in the sequel. It is applicable to solitary waves of all heights, from the highest one with a corner crest of 120° down to very low ones, all with an exponential decrement of the wave profile in the wave outskirt as was first recognized and assumed by Stokes. The UIF-expansion is not a power series, but is consisted of all the intrinsic component functions characterizing the regional properties of the wave field such as the outskirt falling-off rate and the corner crest of the highest wave, both with differing algebraic branch singularities. The solution comes from determining the unknown coefficients of the expansion by optimal minimization of the mean square error of the exact boundary conditions. Thus, the highest wave is

shown to have an amplitude of $\alpha = 0.8331990$ and speed $F = 1.2908904$, with absolute error less than 10^{-6}, involving only fifteen unknowns. Similar results have been obtained for waves down to $\alpha = 10^{-2}$.

However, for the dwarf solitary waves with $\alpha \le 10^{-2}$, the computation required for the UIF-expansion has been found to become so lengthy and complicated that it is unsurmountable down to $\alpha = O(10^{-4})$. Further, longer the wave, much longer spreading the errors. But the accuracy is necessary for accounting of the final stage of wave magnifying to deliver a possibly devastating strike at the ocean bordering destination. In order to get rid of these severe hindrances, Wu and Murashige [5] have introduced a regularized solitary wave theory by applying a conformal transformation of the branch singularities into the so-called regularized coordinates. The present study intends to illustrate applications of this new theory to resolve all the aspects of diminishing dwarf long wave.

2 FORMULATION

2.1 Conformal mapping of the flow domain

Consider a left-going solitary wave in the frame of reference moving with the wave speed c, as shown in Fig.1(a). With the water depth h scaling the length and h/c the time, it is convenient to represent this irrotational plane flow of incompressible and inviscid fluid using the complex velocity w by

$$w = \frac{\mathrm{d}f}{\mathrm{d}z} = u - iv = qe^{i\theta} \tag{1}$$

or the logarithmic hodograph variable ω by

$$w = \tau + i\theta = \log(\frac{1}{w}) \tag{2}$$

where $z = x + iy$ is the complex coordinate and $f = \phi + i\psi$ the complex velocity potential. The wave is bounded above by its free surface at $y = \tilde{y}(x)$ and below by the horizontal channel floor at $y = -1$.

In the *f*-plane, the flow domain lies in the unit strip $-1 \le \psi \le 0$ and $-\infty < \phi < \infty$, as shown in Fig.1(b), and this strip is mapped conformally onto the unit disc $|\zeta| \le 1$ in the ζ-plane, as shown in Fig.1(c), by

$$f + i = \frac{2}{\pi}\lg(\frac{1+\sqrt{\zeta}}{1-\sqrt{\zeta}}) \tag{3}$$

in which the log function and $\sqrt{\zeta}$ are uniquely defined with the branch cut along the positive real ζ-axis ($0 \le \zeta \le 1$), the wave surface is mapped onto the unit circle $|\zeta| = 1$, with the wave crest at $\zeta = -1$, and the channel floor at $\psi = -1$ mapped around the branch cut, reaching the physical infinities at $\zeta = 1 \pm i0$. On the free wave surface,

$$\zeta = e^{i\sigma} \text{ and } \omega = \tau(\sigma) + i\theta(\sigma) \quad (0 < \sigma < 2\pi) \tag{4}$$

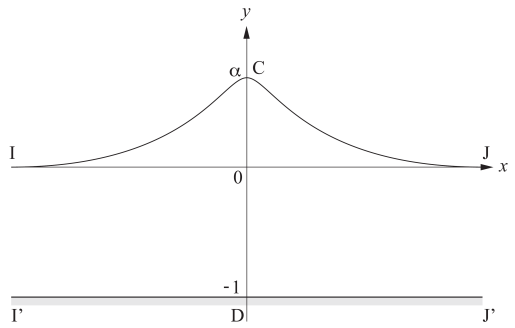

(a) The *z*-plane

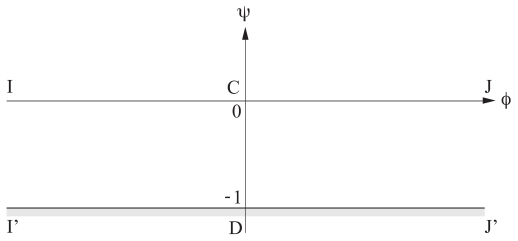

(b) The *f*-plane

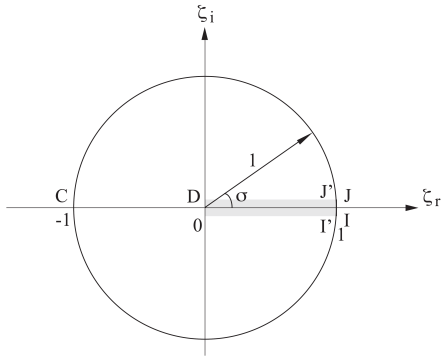

(c) The ζ-plane

Fig.1 Conformal mapping of a solitary wave.

In the ζ-plane, the boundary conditions are given by

$$\pi F^2 e^{-3\tau} \sin(\frac{\sigma}{2})\frac{\partial \tau}{\partial \sigma} + \sin\theta = 0 \quad (0 < \sigma < 2\pi) \tag{5}$$

$$\theta = 0 \quad (\zeta \text{ real}, \ -1 < \zeta < 1) \tag{6}$$

$$\omega = \tau + i\theta \to 0 \quad \text{as} \ \zeta \to +1 \tag{7}$$

where (5) is the gradient of the Bernoulli equation along the wave surface, with Froude number $F = c/\sqrt{gh}$ characterizing the flow, and g being the gravitational acceleration. Thus, solutions can be attained in terms of the conjugate functions τ and θ of $\omega = \tau + i\theta = \omega(\zeta)$ directly under the conditions (5), (6) and (7), as a one-parameter family in Froude number *F*.

2.2 Asymptotic far wave field

The profile of a solitary wave is known, after Stokes, to fall off exponentially, thus with the wave profile and its velocity potential assuming $\tilde{y} = ae^{-ik|x|}$ and $\phi = be^{-k|x|}\cos k(y+h)$ as $x \to \pm\infty$ ($k > 0$ and $a, b \in \Re$). Taking the linear boundary conditions as $\phi_y = \partial\phi/\partial y = cy_x$ and $c\phi_x = -g\tilde{y}$ yields

$$F^2 = \frac{\tan \mu\pi}{\mu\pi} \quad (\mu\pi = kh) \tag{8}$$

which was claimed by Stokes to be exact for all solitary waves (as was verified by Wang and Wu [3]). Thus the Froude number *F* determines the exact value of the exponential decay rate μ.

2.3 The unified intrinsic functional expansion

As stated in Introduction, Wu et al. [1] developed the unified intrinsic functional expansion (UIFE) for $\omega(\zeta)$ in terms of a set of intrinsic component (IC)-functions pertaining to the intrinsic properties of the wave such as the exponential decay in the outskirt. For α of medium down to dwarf solitary waves, the proper UIFE assumes the form

$$\omega(\zeta) = \sum_{m=1}^{M}\sum_{n=0}^{N}[a_{mn}(1+\zeta)^n + b_{mn}\zeta^n](1-\zeta)^{2m\mu} \tag{9}$$

where a_{mn} and b_{mn} are real so that $\theta = 0$ for ζ real to satisfy condition (6), and μ denotes the exponential decay rate given by (8). The terms with $(1-\zeta)^{2m\mu}$ in (9) represent the intrinsic functions on the wave outskirt. Here it is essential that these *M* singular terms with multi-powers of μ in (9) are taken such that 2*M* μ has its integral part of unity, i.e.

$$2M\mu \cong 1 \tag{10}$$

as an ideal criterion for determining $M = M(\mu)$, as emphatically deliberated by Wu et al. [1]. This is necessary to afford an optimally smooth match with the remaining part of ω that is analytic and regular in the vicinity of $\zeta = 1$. However, by this criterion, we should take $M = 30$ for $\alpha = 10^{-3}$, and $M = 90$ for $\alpha = 10^{-4}$. The tasks for evaluation of such dwarf waves by the UIFE (or any) method would be exceedingly tedious and lengthy. It is therefore of great significant to develop a new innovative scheme for effective resolution of all the dwarf solitary waves.

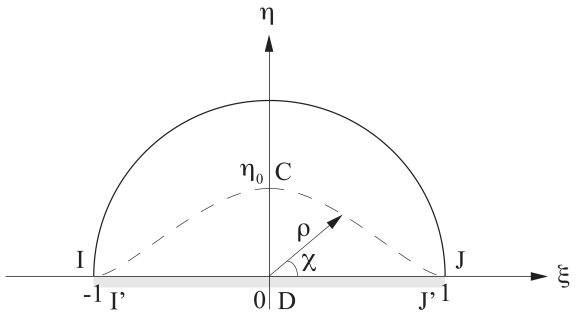

Fig. 2 Regularized coordinates (the *t*-plane). $t = \xi + i\eta$. The dashed line represents the wave surface

3 REGULARIZED COORDINATES

3.1 Conformal mapping for regularization

By Wu and Murashige [5], the regularized coordinate, namely $t = \xi + i\eta = \rho e^{i\chi}$, is given by the conformal transformation:

$$1 - t^2 = (1-\zeta)^{2\mu} \tag{11}$$

with the same branch cut for (3). Figure 2 shows the flow field in the *t*-plane. This conformal map $t = t(\zeta)$ of (11) has the following basic properties.

(i) For $\zeta = -1$ at the wave crest, we readily find

$$t(-1) = i\eta = i(2^{2\mu} - 1)^{1/2} \equiv i\eta_0 \tag{12}$$

which is located at the crest of a gentle mount, fore-and-aft symmetric between the two foothill ends at $\zeta = \pm 1$ as the mapped image of the solitary wave profile in Fig.3. The mount height η_0 decreases with the wave height, $\eta_0 \to (2\mu\log 2)^{1/2}$ as $\mu \to 0$.

(ii) In the neighborhood of the physical infinity $t = 1$,

$|1-t|<<1$, relation (11) can be written as

$$2(1-t) = (1-\zeta)^{2\mu} + O(|1-t|^2) \tag{13}$$

and

$$\arg(1-t) = 2\mu \arg(1-\zeta) \tag{14}$$

On the wave outskirt $\zeta = e^{i\sigma}$ ($0 < \sigma << 1$), we have

$$\arg(1-t) = 2\mu \arg(1-e^{i\sigma}) = -\mu(\pi - \sigma) \tag{15}$$

which is convex to the slope angle $-\mu\pi$ for dwarf waves, diminishing with wave height as $\mu \to 0$.

For a generic point $\zeta = e^{i\sigma}$ on the wave surface, $(1-\zeta)^{2\mu}$ in (11) can be expressed as

$$(1-e^{i\sigma})^{2\mu} = A(\sigma)e^{-i\beta(\sigma)} \tag{16}$$

where

$$\begin{aligned} A(\sigma) &= (2\sin\frac{\sigma}{2})^{2\mu}, \\ \beta(\sigma) &= \mu(\pi - \sigma), \end{aligned} \tag{17}$$

and, from these, we get

$$A = (2\cos\frac{\beta}{2\mu})^{2\mu} \tag{18}$$

Using this relation and substituting $t = \xi + i\eta$ into $(1-t^2)$ in (11), we can determine the conformal image of solitary wave profile $\eta = \tilde{\eta}(\xi)$ in the *t*-plane as shown in Fig.3. In addition, using $\eta = \tilde{\eta}(\xi)$, we can obtain $\hat{A}(\xi) = A(\sigma(\xi))$ and $\hat{\beta}(\xi) = \beta(\sigma(\xi))$ as

$$\begin{aligned} \hat{A}(\xi) &= \sqrt{1 - 2(\xi^2 - \tilde{\eta}^2) + (\xi^2 + \tilde{\eta}^2)^2} \\ \hat{\beta}(\xi) &= \tan^{-1}\frac{2\xi\tilde{\eta}}{1 - (\xi^2 - \tilde{\eta}^2)} \end{aligned} \tag{19}$$

We need $dt/d\sigma$ to derive the free surface condition in the *t*-plane. Taking differentiation of both sides of $1 - t^2 = Ae^{-i\beta}$ with respect to σ, we get

$$\frac{\mathrm{d}t}{\mathrm{d}\sigma} = \frac{\mathrm{d}\xi}{\mathrm{d}\sigma} + i\frac{\mathrm{d}\eta}{\mathrm{d}\sigma} = -\frac{1}{2t}(\frac{\mathrm{d}A}{\mathrm{d}\sigma} - iA\frac{\mathrm{d}\beta}{\mathrm{d}\sigma})e^{-i\beta} \tag{20}$$

where, from (17), $\mathrm{d}A/\mathrm{d}\sigma$ and $\mathrm{d}\beta/\mathrm{d}\sigma$ are given by

$$\begin{aligned} \frac{\mathrm{d}A}{\mathrm{d}\sigma} &= \mu 2^{2\mu}(\sin\frac{\sigma}{2})^{2\mu-1}\cos\frac{\sigma}{2}, \\ \frac{\mathrm{d}\beta}{\mathrm{d}\sigma} &= -\mu \end{aligned} \tag{21}$$

Here we note that $2\mu < 1$ for all solitary waves ($\mu \le \mu_{\max} = 0.33506$ for the highest solitary wave). Hence $\mathrm{d}A/\mathrm{d}\sigma \to \infty$ as $\sigma \to 0$. To this point, it should be simpler to adopt the cartesian coordinate ξ as the independent variable, for $\mathrm{d}\eta/\mathrm{d}\xi$ is uniformly regular over the entire wave surface as we have noted above. In particular, using (19) and $\beta = \mu\pi$ at the physical infinity $\sigma = 0$ or $\xi = 1$, we obtain

$$\left.\frac{\mathrm{d}\tilde{\eta}}{\mathrm{d}\xi}\right|_{\xi=1} = \tilde{\eta}'(1) = -\tan\mu\pi \tag{22}$$

Thus, as $\xi \to 1$,

$$\begin{aligned} \hat{A}(\xi) &= 2\sqrt{1 + \tilde{\eta}'(1)^2}(1-\xi) + O(|1-\xi|^2) \\ &= \frac{2}{\cos\mu\pi}(1-\xi) + O(|1-\xi|^2) \end{aligned} \tag{23}$$

These results exemplify the regularization.

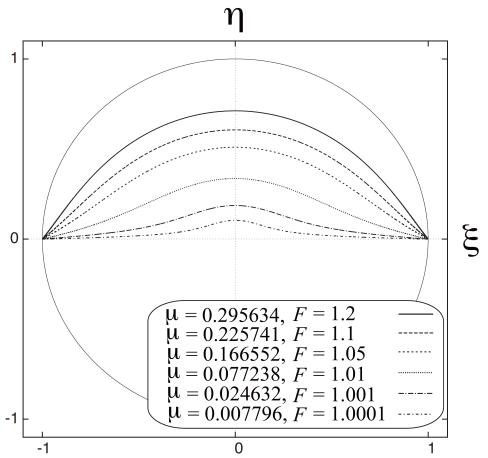

Fig.3 Conformal images of solitary wave profiles $\eta = \tilde{\eta}(\xi)$ in the regularized *t*-plane. $t = \xi + i\eta$
μ : the exponential decay rate in (8),
F : the Froude number

The free surface condition expressed in terms of the independent variable ξ in the *t*-plane becomes, for $-1 < \xi < 1$,

$$G(\xi) = -\mu\pi F^2 g(\xi) e^{-3\tau} \frac{\partial \tau}{\partial \xi} + \sin\theta = 0 \qquad (24)$$

with

$$g(\xi) = \frac{1}{2}\{\frac{1}{\rho}\sin(\chi + \frac{\hat{\beta}}{2\mu}) + \rho\sin(\chi - \frac{\hat{\beta}}{2\mu})\} \qquad (25)$$

where $t = \xi + i\tilde{\eta}(\xi) = \rho(\xi)e^{i\chi(\xi)}$, with

$$\rho(\xi) = \sqrt{\xi^2 + \tilde{\eta}(\xi)^2}\ ,$$
$$\chi(\xi) = \tan^{-1}\frac{\tilde{\eta}(\xi)}{\xi} \qquad (26)$$

3.2 Expansion of ω in the t-plane

In the regularized t-plane, $\omega = \omega(t)$ can be expanded in the form

$$\omega(t) = \sum_{n=1}^{\infty} a_n (1 - t^{2n}) \qquad (27)$$

where the unknown coefficients a_n's are real. This expansion form satisfies the channel floor condition $\theta = 0$ for $-1 < \xi < 1$ on the real t-axis, and the physical infinity condition $\omega(t) \to 0$ as $t \to \pm 1$. Furthermore, near the physical infinity $t = 1$, $|1 - t| << 1$, we have (13) and

$$1 - t^{2n} = 2n(1 - t) + O(|1 - t|^2) \qquad (28)$$

Hence we can show that the expansion form (27) can satisfy the free surface condition (24) locally near the physical infinities $t = \pm 1$.

Using (26), we can write (27) as

$$\omega(t = \xi + i\eta(\xi)) = \tau(\xi) + i\theta(\xi) \qquad (29)$$

with

$$\tau(\xi) = \sum_{n=1}^{\infty} a_n B_{\tau,n}(\xi)\ ,$$
$$\theta(\xi) = \sum_{n=1}^{\infty} a_n B_{\theta,n}(\xi) \qquad (30)$$

and

$$B_{\tau,n}(\xi) = 1 - \rho(\xi)^{2n}\cos 2n\chi(\xi) \qquad (31a)$$

$$B_{\theta,n}(\xi) = -\rho(\xi)^{2n}\sin 2n\chi(\xi) \qquad (31b)$$

4 THE METHOD OF COMPUTATION

The basic idea of the computational method is the same as that in [1]. That is, the series expansions (30) of $\tau(\xi)$ and $\theta(\xi)$ are truncated with N terms, and the N unknown coefficients $a_n^{'s}$ are iteratively determined by minimizing the mean-square error E of the only condition (24)-(25) left on the entire wave surface

$$E(\mathbf{a}) = \| G \|_2 = (\int_0^1 G(\xi;\mathbf{a})^2 \mathrm{d}\xi)^{1/2} \qquad (32)$$

where $\boldsymbol{a} = (a_1, a_2, \cdots, a_N)$. For minimization, we applied Newton's method for

$$H_k(\mathbf{a}) = \frac{1}{2}\frac{\partial E^2}{\partial a_k} = \int_0^1 G(\xi;\mathbf{a})\frac{\partial G}{\partial a_k}\mathrm{d}\xi = 0$$
$$(k = 1,2,\cdots,N) \qquad (33)$$

As an index of error, we adopt the relative error

$$\frac{\| G \|_2}{\| \boldsymbol{a} \|_{\max}} = \frac{E}{\max\limits_{1 \le n \le N} |a_n|} \qquad (34)$$

This is also used in the stopping condition of Newton's method.

In real computations, it was found that convergence of this iterative method gets worse with increase of N, because neither of the base functions $\{B_{\tau,n}\}$ and $\{B_{\theta,n}\}$ in (31) is orthogonal by itself. Hence $\{B_{\theta,n}\}$ is orthonormalized using the Schmidt transformation, and correspondingly $\{B_{\tau,n}\}$ is transformed.

In addition, the sample points $\xi_j (j = 0,1,\cdots,J)$ on the interval [0,1] are distributed such that resolution near the physical infinity $\xi = 1$ is enough for numerical integration, using the geometric sequence as

$$\xi_j = 1 - \upsilon^j \Delta\xi_0 \quad (j = 1,2,\cdots,J-1) \qquad (35)$$

with $\xi_0 = 1$ and $\xi_J = 1$. Here $\upsilon > 1$ and $0 < \Delta\xi_0 << 1$ are chosen such that $\upsilon^J \Delta\xi_0 = 1$.

The algorithm of this computational method can be summarized as follows:

Step 1
Set the Froude number F, the number N of terms of the truncated expansion (30), the number J of sample points ξ_j and the minimum interval $\Delta\xi_0$ in (35). Distribute the sample points $\xi_j (j = 0,1,\cdots,J)$ on the interval [0,1] using (35).

Step 2
Fix the exponential decay rate μ using Stokes' relation (8).

Step 3
Compute $\tilde{\eta}(\xi_j)$ using (11) and (18), and $\rho(\xi_j)$ and $\chi(\xi_j)$ using (26).

Step 4
Compute the base functions $B_{\tau,n}(\xi_j)$ and $B_{\theta,n}(\xi_j)$ ($j = 0,1,\cdots,J$ and $n = 1,2,\cdots,N$) using (31), and transform them using the Schmidt method.

Step 5
Iteratively determine a_n's using Newton's method for (33). The trapezoidal rule is used for numerical integration.

Step 6
If the condition $\| G \|_2 / \| \mathbf{a} \|_{\max} < \varepsilon (= 10^{-10})$ is satisfied, then stop the computation. Otherwise, increase N and go to Step 4.

Note that, in order to reduce the round-off errors, orthonormalization using the Schmidt transformation in step 4 was performed with the multiple precision arithmetic using the library ``exflib" [6] which enables us to arbitrarily increase the number of significant digits. The other computations were executed with the double precision.

5 THE COMPUTED RESULTS

Table 1, Figs.4 and 5 show some computed results. In these numerical examples, the number J of sample points ξ_j and the minimum interval $\Delta\xi_0$ are fixed to $J = 3000$ and $\Delta\xi_0 = 10^{-5}$, respectively. Iteration of Newton's method was stopped when $\| G \|_2 / \| \boldsymbol{a} \|_{\max} < 10^{-10}$ was satisfied.

Table 1 summarizes the computed results of the amplitude-to-water depth ratio $\alpha = a/h$ for $1.0005 \le F \le 1.03$ with the number N of terms in the series expansion and the relative error $\| G \|_2 / \| \boldsymbol{a} \|_{\max}$. It is found that accurate enough results with the relative error $< 10^{-10}$ are obtained even for $\alpha \cong 10^{-3}$.

Figure 4 shows the computed results of τ and θ for F = 1.0005, 1.001 and 1.003. Note that $\xi = 1$ or $\sigma = 0$ corresponds to the physical infinity, and $\xi = 0$ or $\sigma = \pi$ the wave crest. We can see that $\tau(\sigma)$ and $\theta(\sigma)$ change very sharply with σ near $\sigma = 0$, but that variation of $\tau(\xi)$ and $\theta(\xi)$ with ξ in the regularized coordinates is smooth even near $\xi = 1$.

We can obtain the wave profile using

$$x(\xi) = \frac{1}{\mu\pi}\int_0^{\xi} e^{\tau(\xi)} \cos\theta(\xi) \frac{1}{g(\xi)} \mathrm{d}\xi,$$
$$\tilde{y}(\xi) = -\frac{1}{\mu\pi}\int_{\xi}^{1} e^{\tau(\xi)} \sin\theta(\xi) \frac{1}{g(\xi)} \mathrm{d}\xi, \tag{36}$$

where $g(\xi)$ is given by (25). The amplitude-to-water depth ratio $\alpha = a/h$ is determined using

$$\alpha = -\frac{1}{\mu\pi}\int_0^{1} e^{\tau(\xi)} \sin\theta(\xi) \frac{1}{g(\xi)} \mathrm{d}\xi, \tag{37}$$

Figure 5 shows the wave profiles $y = \tilde{y}(x)$ for F = 1.0005, 1.001 and 1.003. We can find that the wave elevation for smaller Froude number is lower than that for larger Froude number near the wave crest, but is higher in the outskirts.

In addition, we calculated the integral properties of dwarf solitary waves, namely the excess mass M, the potential and kinetic energy E_p and E_k and the net circulation Γ. In the regularized coordinates, these are given by

$$M = \frac{2F^2}{\mu\pi}\int_0^{1} \sinh\tau(\xi) \frac{\cos\theta(\xi)}{g(\xi)} \mathrm{d}\xi, \tag{38}$$

$$E_P = \frac{F^4}{\mu\pi}\int_0^{1} e^{-\tau(\xi)} \sinh^2\tau(\xi) \frac{\cos\theta(\xi)}{g(\xi)} \mathrm{d}\xi, \tag{39}$$

$$E_K = \frac{F^4}{\mu\pi}\int_0^{1} \sinh\tau(\xi) \frac{(\cos\theta(\xi) - e^{-\tau(\xi)})}{g(\xi)} \mathrm{d}\xi, \tag{40}$$

$$\Gamma = \frac{2F}{\mu\pi}\int_0^{1} \frac{(e^{\tau(\xi)} \cos\theta(\xi) - 1)}{g(\xi)} \mathrm{d}\xi, \tag{41}$$

We can examine accuracy of these computed results

using Starr's identity

$$I_S = E_P - \frac{(F^2-1)M}{3} = 0 \tag{42}$$

and McCowan's identity

$$I_M = E_K - \frac{F(FM-\Gamma)}{2} = 0 \tag{43}$$

Table 2 shows that the computed results satisfy these identities with enough accuracy. Figure 6 compares the kinetic energy density $\mathrm{d}E_k/\mathrm{d}\xi$ with the approximate solutions by the Friedrichs-Hyers equation [4] which is derived from the 1st order theory. It is found that accurate computations are required even for low solitary waves.

6 CONCLUSIONS

We have considered accurate computation of dwarf solitary waves of which the amplitude-to-water depth ratio $\alpha \le 10^{-2}$. In this computation, it is critical to suitably deal with singular behaviour of flow variables near the physical infinities $|x| \to \infty$. This work introduced regularized coordinates in which the flow domain is conformally mapped and the physical infinities are not singular. In the regularized t-plane, the logarithmic hodograph variable $\omega = \omega(t)$ is analytic and can be expanded in a Taylor series form. We developed a computational method to iteratively determine unknown coefficients of the series expansion. Numerical examples demonstrate that the proposed method can produce accurate enough solutions even for $\alpha \cong 10^{-3}$ or less.

ACKNOWLEDGEMENTS

We wish to express our cordial thanks to Dr. Yoshitaka Watanabe of Kyushu University for his valuable advice on numerical calculation. This work was partly supported by Grants-in-Aid for Scientific Research (S) No.20224001.

Table 1 Computed results of the amplitude-to- water depth ratio $\alpha = a/h$ and the relative error $\|G\|_2 / \|\mathbf{a}\|_{\max}$.
N : the number of terms in the series expansion,
F : the Froude number

F	N	α	$\|G\|_2/\|\boldsymbol{a}\|_{\max}$
1.0005	42	1.000300×10^{-3}	1.09×10^{-11}
1.001	34	2.001201×10^{-3}	3.93×10^{-11}
1.003	30	6.010818×10^{-3}	3.04×10^{-12}
1.005	26	1.003007×10^{-2}	1.01×10^{-11}
1.01	22	2.012060×10^{-2}	3.09×10^{-11}
1.025	30	5.075968×10^{-2}	4.11×10^{-11}
1.03	34	6.109694×10^{-2}	5.85×10^{-12}

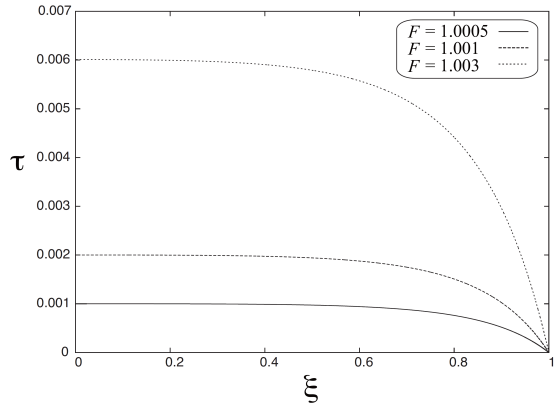

(a.1) $\tau(\xi)$

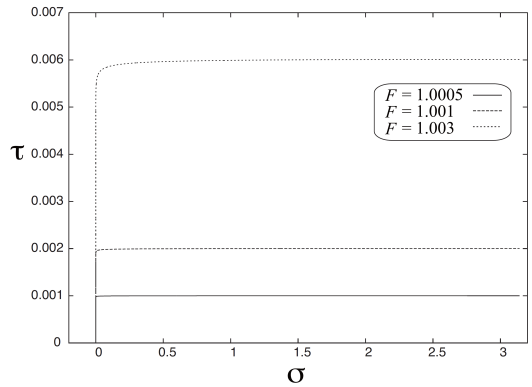

(a.2) $\tau(\sigma)$

Fig.4 Computed results of τ and θ using the regularized coordinates for F = 1.0005, 1.001 and 1.003
$\xi = 1$ ($\sigma = 0$) : the physical infinity,
$\xi = 0$ ($\sigma = \pi$) : the wave crest.

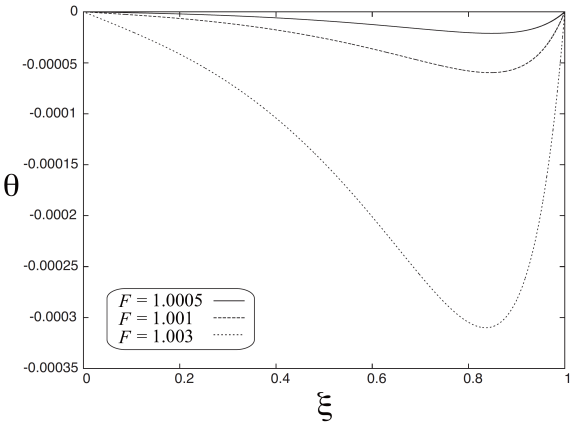

(b.1) $\theta(\xi)$

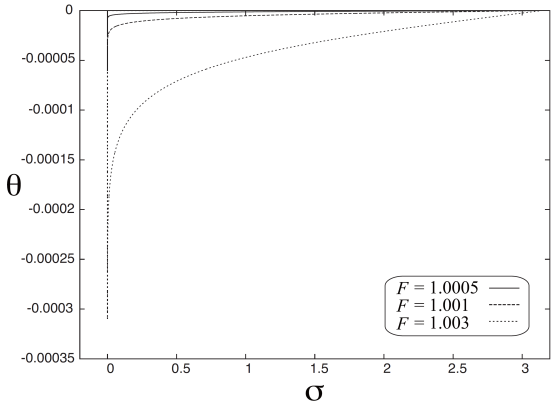

(b.2) $\theta(\sigma)$

Fig.4 (continue) Computed results of τ and θ using the regularized coordinates for F = 1.0005, 1.001 and 1.003

$\xi = 1$ ($\sigma = 0$) : the physical infinity,

$\xi = 0$ ($\sigma = \pi$) : the wave crest

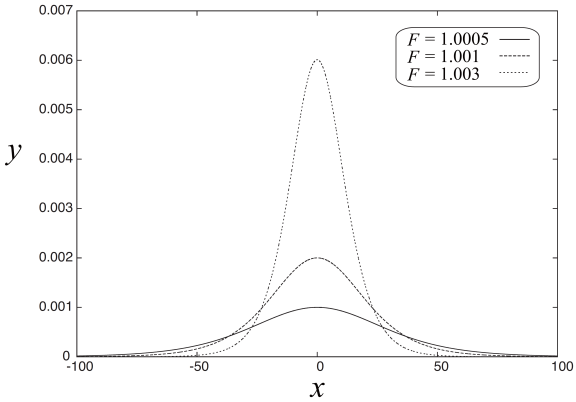

Fig.5 Wave profile $y = \tilde{y}(x)$ for F = 1.0005, 1.001 and 1.003

Table 2 The computed results of the excess mass M, the potential energy E_P, the kinetic energy E_K and the circulation Γ. (I_S : (42) and I_M : (43).)

(a) E_P and E_K

F	E_P	E_K
1.0005	2.436210×10^{-5}	2.437184×10^{-5}
1.001	6.895979×10^{-5}	6.901493×10^{-5}
1.003	3.594351×10^{-4}	3.602963×10^{-4}
1.005	7.757698×10^{-4}	7.788638×10^{-4}
1.01	2.211108×10^{-3}	2.228694×10^{-3}
1.03	1.184098×10^{-2}	1.212030×10^{-2}

(β) M and Γ

F	M	Γ
1.0005	7.306804×10^{-2}	7.305585×10^{-2}
1.001	1.033880×10^{-1}	1.033535×10^{-1}
1.003	1.794484×10^{-1}	1.792683×10^{-1}
1.005	2.321505×10^{-1}	2.317613×10^{-1}
1.01	3.300161×10^{-1}	3.289030×10^{-1}
1.03	5.832997×10^{-1}	5.772641×10^{-1}

(c) $|I_S|$ and $|I_M|$

F	$\lvert I_S \rvert$	$\lvert I_M \rvert$
1.0005	1.69×10^{-12}	2.54×10^{-12}
1.001	5.02×10^{-12}	7.55×10^{-12}
1.003	2.43×10^{-11}	3.67×10^{-11}
1.005	5.68×10^{-11}	8.60×10^{-11}
1.01	1.90×10^{-10}	2.90×10^{-10}
1.03	1.27×10^{-9}	2.02×10^{-9}

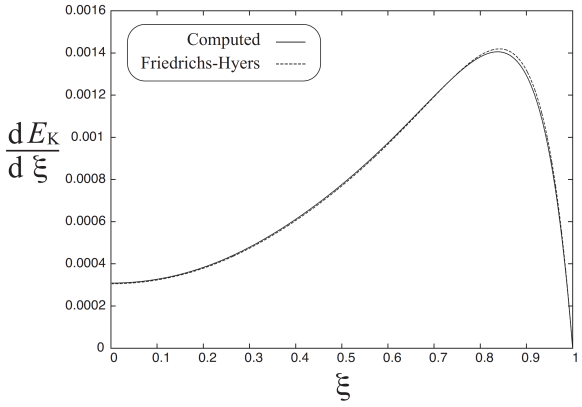

(a) F=1.005

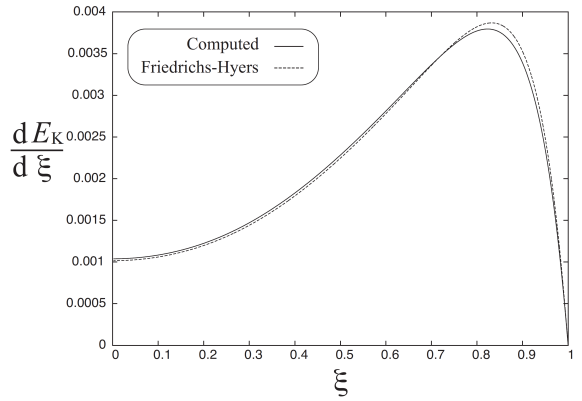

(b) F=1.01

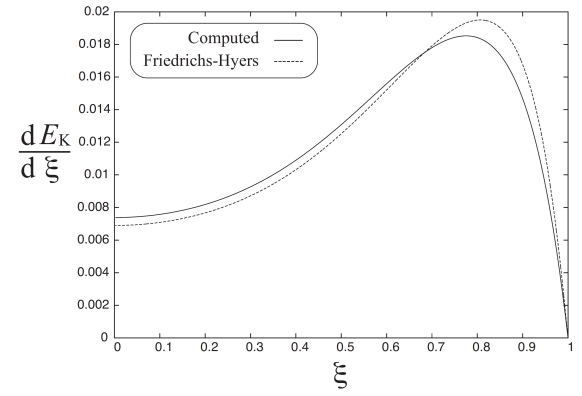

(c) F=1.03

Fig.6 Comparison of the computed results of the kinetic energy density $dE_K/d\xi$ with the approximate solutions of the Friedrichs-Hyers equation [4]. ξ=0 : the wave crest and ξ =1 : the physical infinity

REFERENCES

[1] Wu TY, Kao J, Zhang J E. A unified intrinsic functional expansion theory for solitary waves. Acta Mech Sinica, 2005, 21:1-15.
[2] Wu T Y, Wang X, Qu Q. On solitary waves. Part 2. A unified perturbation theory for higher-order waves. Acta Mech Sinica, 2005, 21: 515-530.
[3] Wang X L, Wu T Y. Integral convergence of the higher-order theory for solitary waves. Physics Letters A., 2006, 350: 44-50.
[4] Friedrichs K O, Hyers D H. The existence of solitary waves. Commun. Pure Appl. Math., 1954,7:517-550.
[5] Wu T Y, Murashige S. On tsunami and the regularized solitary wave theory. (To appear in J. Eng. Math.)
[6] http://www-an.acs.i.kyoto-u.ac.jp/~fujiwara/exflib/